Ground motions in New Zealand from Kermadec megathrust earthquakes

B Fry
K Gledhill
R Benites

GNS Science Report 2018/33
October 2018

DISCLAIMER

The Institute of Geological and Nuclear Sciences Limited (GNS Science) and its funders give no warranties of any kind concerning the accuracy, completeness, timeliness or fitness for purpose of the contents of this report. GNS Science accepts no responsibility for any actions taken based on, or reliance placed on the contents of this report and GNS Science and its funders exclude to the full extent permitted by law liability for any loss, damage or expense, direct or indirect, and however caused, whether through negligence or otherwise, resulting from any person's or organisation's use of, or reliance on, the contents of this report.

BIBLIOGRAPHIC REFERENCE

Fry B, Gledhill K, Benites R. 2018. Ground motions in New Zealand from Kermadec megathrust earthquakes. Lower Hutt (NZ): GNS Science. 17p. (GNS Science report; 2018/33). doi:10.21420/7J43-G338.

B Fry, GNS Science, PO Box 30 368, Lower Hutt 5040, New Zealand
K Gledhill, GNS Science, PO Box 30 368, Lower Hutt 5040, New Zealand
R Benites, GNS Science, PO Box 30 368, Lower Hutt 5040, New Zealand

www.gns.cri.nz

ISSN 2350-3424 (online)
ISBN 978-1-98-856903-1 (online)
http://dx.doi.org/10.21420/7J43-G338

CONTENTS

ABSTRACT ..... **III**

KEYWORDS ..... **III**

1.0 INTRODUCTION **1**

1.1 Ground Motions from Kermadec Earthquakes 1

1.1.1 Azimuthally dependent source radiation 1

1.1.2 Geometric spreading 3

1.1.3 Anelastic attenuation 4

2.0 GROUND MOTION SIMULATIONS **7**

3.0 CONCLUSIONS **9**

4.0 ACKNOWLEDGMENTS **10**

5.0 REFERENCES **10**

FIGURES

Figure 1.1 Example seismograms showing dominant energy radiation in the direction perpendicular to a thrust fault. 2

Figure 1.2 White inset is a representation of the radiation pattern of two modes of seismic waves radiating out from a scenario earthquake originating on the southern Kermadec Subduction zone. 3

Figure 1.3 Ground motions for an M8.5 subduction zone earthquake as calculated from empirical ground motion prediction equations derived from fitting global observations. 4

Figure 1.4 Map showing anelastic attenuation (inverse of “quality” (Q)) for New Zealand from Eberhart-Phillips and Fry, (2018). 5

Figure 1.5 Left panel: Felt reports overlain by predicted regions of felt intesity from the September 2018 M6.9 Kermadec earthquake. 6

Figure 2.1 Left panel: Results from AxiSEM simulations of M8.5 earthquakes along the Kermadec Subduction zone. 7

Figure 2.2 Comparison of our AxiSEM results with the recent ground motion prediction equation of Abrahamson et al., 2016. 8

APPENDICES

A1.0 NUMERICAL SIMULATIONS **13**

A1.1 AxiSEM modelling 13

A1.2 Discrete Wavenumber modelling 14

APPENDIX FIGURES

Figure A1.1 P and S velocity profiles (left panel) and Qp and Qs attenuation models (right panel) used in AxiSEM and discrete wavenumber numerical simulation. 13

Figure A1.2 Peak ground displacement from our simulations as a function of distance from Tauranga. 14
Figure A1.3 Intensity table showing classification scheme used to assess perceived shaking against peak ground motions. 14
Figure A1.4 Results of the southernmost M8.5 simulation shown in figure 2.1. 17

ABSTRACT

We use numerical simulations of earthquake ground shaking to test the ability of natural warning to trigger self-evacuation in communities in the north-western North Island that are at risk of tsunami generated along the Kermadec Subduction Zone in the southwest Pacific. In this region, self-evacuation defined as “Long or Strong, Get Gone” is the dominant mechanism for risk mitigation. However, we conclude that many possible earthquakes will not be felt strongly in these regions, including densely populated metropolitan areas on the coast from the Bay of Plenty to Northland, such as the cities of Tauranga, Auckland and Whangarei. These earthquakes could then cause tsunami waves with maximum wave amplitudes in excess of 5m within the first hour after the earthquake. This finding suggests that reliance on self-evacuation alone must be supplemented with scientific monitoring and alerting mechanisms to protect vulnerable populations.

KEYWORDS

Kermadec Subduction zone, megathrust earthquake, tsunami, subduction ground motions

1.0 INTRODUCTION

The 2004 Sumatran earthquake and subsequent tsunami triggered global efforts to implement effective tsunami early warning in the world's major tsunami-prone ocean basins. Tsunami early warning for earthquake generated tsunami typically involves using seismic observations of the causal earthquake to estimate the size of the tsunami that was generated and then forecasting the resulting impacts in coastal regions. This forecasting process is iteratively refined as further data is available from ocean observations. This effort is still ongoing and rapid advances are still continuing. Numerous promising techniques based on ocean elevation, atmospheric disturbance, and ground deformation are currently being validated and will likely find use in the coming decades. These methods are dominantly useful for regional or distant earthquakes in which tsunami travel times are greater than a few hours, and in some cases, local earthquakes that occur near to terrestrial observational networks. However, even with accurate rapid forecasts of approaching waves, short tsunami travel times from local earthquakes make warnings difficult to communicate to affected communities. In these situations, self-evacuation triggered by natural warning remains the best option for risk reduction. Natural warning is typically the perception, or "felt intensity" of strong ground motion at affected coastlines.

Unfortunately, there exists a class of regional earthquakes that falls through the New Zealand early warning net. These are events that occur close enough to affected coasts to yield travel times of less than an hour yet are far enough away that terrestrial observation networks are inadequate to forecast tsunami impacts accurately. An outstanding question is whether these events will be felt strongly enough to trigger natural warning based self-evacuation. To answer this question, we simulate ground motions from subduction earthquake scenarios along the Kermadec subduction zone. We show that plausible large Kermadec subduction zone earthquakes are capable of generating damaging tsunamis that can reach New Zealand coastlines within an hour of the earthquake, yet will likely not be strongly felt in many potentially affected communities.

1.1 Ground Motions from Kermadec Earthquakes

In this report, we focus on understanding ground motions from M8.5 earthquake scenarios occurring along the Kermadec subduction zone megathrust fault from north of East Cape to the Louisville Ridges. We calculate hard-rock ground motions in Tauranga as a proxy for felt intensity for the north coast of the North Island from the Bay of Plenty through to the coastal northwestern North Island. We use sophisticated numerical modeling to examine the impact of 3 distinct effects on the nature of ground motion intensities. These are 1) directional radiation of energy from the earthquake source, 2) geometrical spreading of the earthquake waves as they travel away from the earthquake, and 3) anelastic attenuation of seismic waves as they pass through the highly attenuating Havre Trough and Taupo Volcanic Zone.

1.1.1 Azimuthally dependent source radiation

When an earthquake occurs, seismic energy does not radiate outward in a homogenous fashion. Rather, the amount of energy released is dependent on orientation of the fault plane and mechanics of the earthquake. Directional radiation of ground shaking from thrust faults tends to concentrate most of the energy perpendicular to the strike of the fault (Figure 1.1).

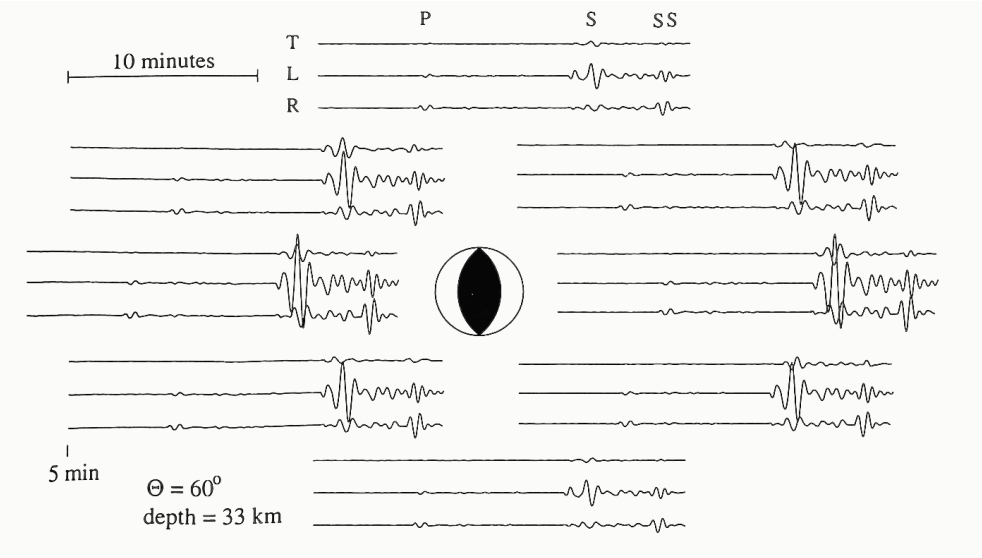

Figure 1.1 Example seismograms showing dominant energy radiation in the direction perpendicular to a thrust fault. The 'beach ball' represents a thrust fault oriented north-south. The surrounding seismograms (oriented in map view) clearly show most energy (largest waves) travelling east-west. Figure from Aki and Richards, 2002.

Megathrust earthquakes along the Kermadec Subduction zone tend to focus much of their energy, and consequently strongest ground shaking, in a northwest-southeast direction (Figure 1.2). Most of their energy will be directed away from New Zealand.

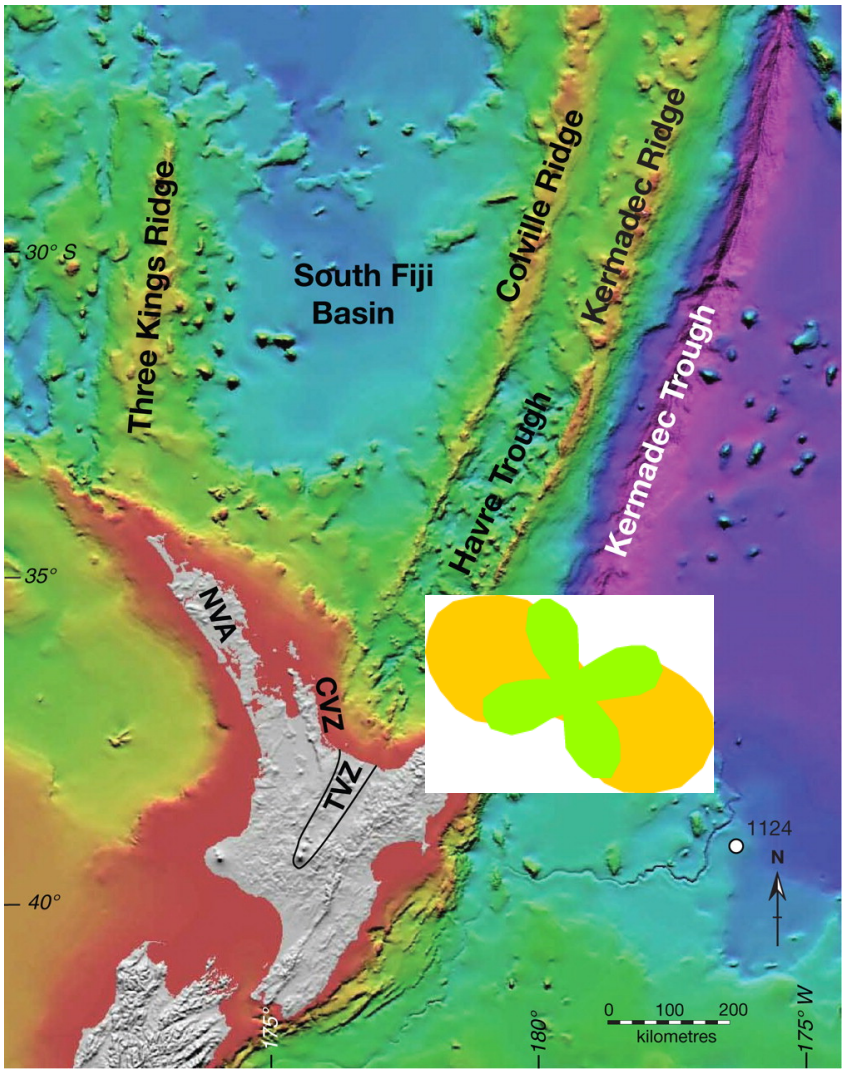

Figure 1.2 White inset is a representation of an example of the radiation pattern of two modes of seismic waves radiating out from a scenario earthquake originating on the southern Kermadec Subduction zone. Other modes are also oriented in a similar way. Yellow and green lobes show the primary patterns of maximum energy of seismic surface waves travelling away from the earthquake. Note that most energy coming from Kermadec sources is dominantly sent in northwest-southeast directions, away from New Zealand. "TVZ" represents the Taupo Volcanic Zone. Havre Trough is the extension of the TVZ offshore. Both of these features influence ground motions and will be discussed in Section 1.1.3.

1.1.2 Geometric spreading

After energy has been released from the earthquake, it travels away from the source. Depending on the type of wave, its energy decreases rapidly with increasing to epicentral distance. This means that ground shaking decays rapidly with increasing distance from the earthquake rupture (Figure 1.3). A conventional tsunami-causing earthquake can therefore often simply occur too far away to be felt strongly. Tsunami waves, however, are able to be transmitted long distances with very little loss of energy, making them dangerous to coastlines even far from the source, including the sources from much of the Kermadec subduction zone, and the Tonga and New Hebrides subduction zones.

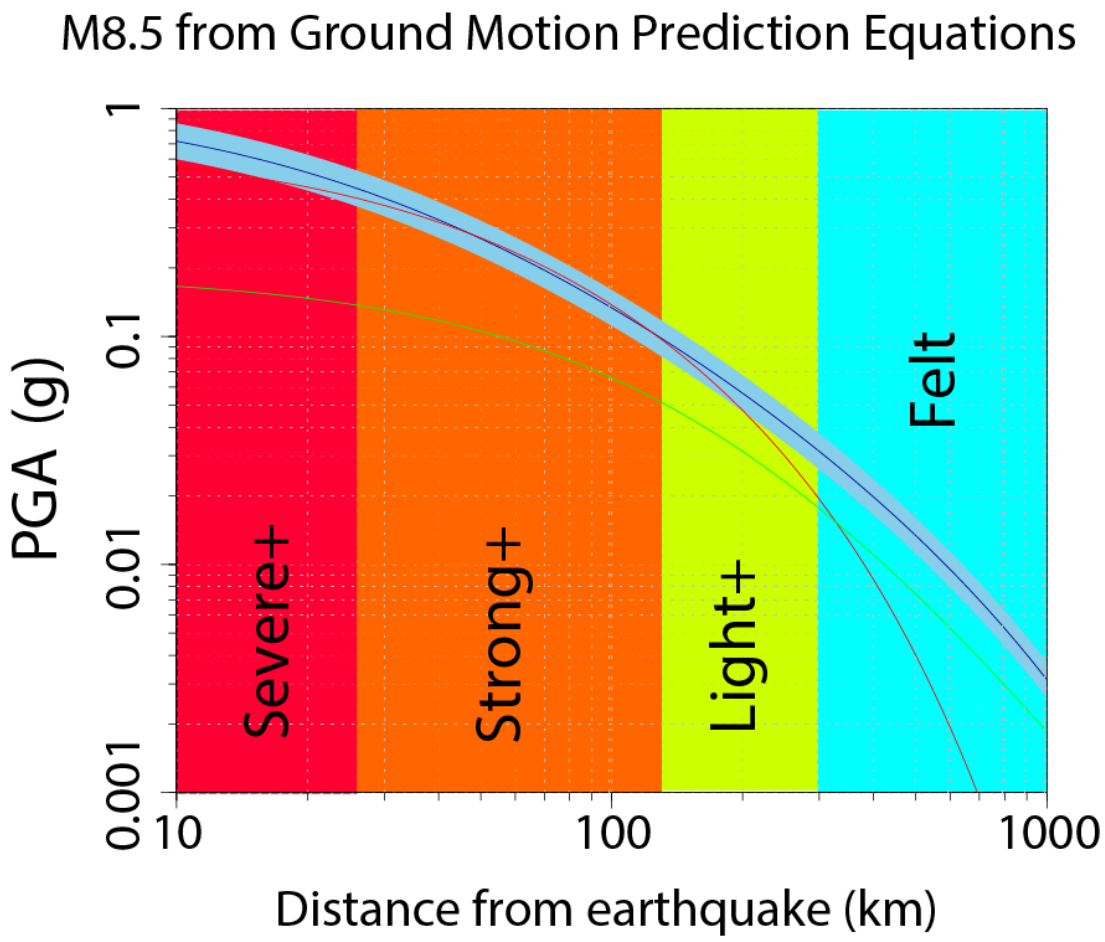

Figure 1.3 Ground motions for an M8.5 subduction zone earthquake as calculated from empirical ground motion prediction equations derived from fitting global observations. Models are blue (Abrahamson et al., 2016), green (Atkinson and Boore, 2003; 2006), and Zhao et al, 2006 (red). Distances have been colour coded according to felt intensities from Worden et al., (2012). Note, observational evidence suggests that, on average, global subduction zone earthquakes of this magnitude are not strongly felt after about 150km from the source. These simple calculations do not account for radiation patterns or New Zealand specific attenuation as presented in section 2 of this report.

1.1.3 Anelastic attenuation

Due to volcanic processes driven by subduction of the Pacific Plate at the Hikurangi and Kermadec margins, the Taupo Volcanic Zone and Havre Trough (see Figure 1.2 for location) are highly attenuating, or inefficient at transmitting seismic wave energy. As seismic waves pass through these regions, they lose amplitude at a faster rate than usual. This compounds the effect of geometric spreading as described above, making most tsunamigenic earthquakes along the Kermadec Subduction zone unlikely to be strongly felt in many tsunami-prone coastal areas of the northwestern North Island of New Zealand. Recent work has improved our understanding of this attenuation pattern (Figure 1.4, Eberhart-Phillips and Fry, 2018) in New Zealand, which we can assume extends farther to the north along the Havre Trough.

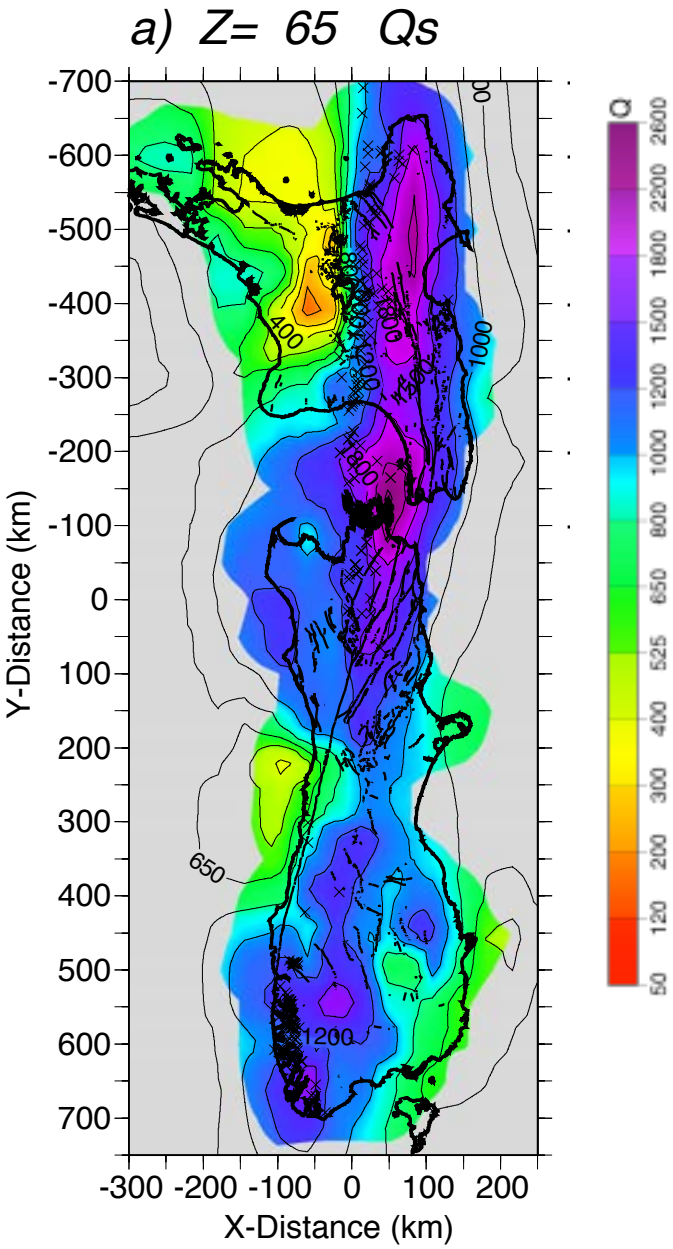

Figure 1.4 Map showing quality (Q), which is the inverse of attenuation for New Zealand from Eberhart-Phillips and Fry, (2018). Regions in cool colours mark efficient propagation of seismic waves, with relatively little loss of energy with distance travelled. Areas in warm colours mark inefficient propagation of seismic waves, with relatively high loss of energy with distance travelled. Yellows and greens corresponding to the TVZ and Havre Trough reduce much of the seismic energy from earthquakes occurring on the Kermadec Subduction zone prior to arrival in the western North Island.

Recently, an M6.9 earthquake on 10 September 2018, with an epicentre approximately 600km north of the North Island along the Kermadec Subduction zone provided a ground-truth validation of this attenuation model. GeoNet recorded over 2000 felt reports in New Zealand (Figure 1.4). However, even with the large population of the greater Auckland/Whangarei/Tauranga region, only one felt report was received from the north-western North Island. The location and density of felt reports and the low attenuation areas from the map presented in Figure 1.4 are notably correlated (Figure 1.5). This is strong validation of our numerical results presented in Section 2.

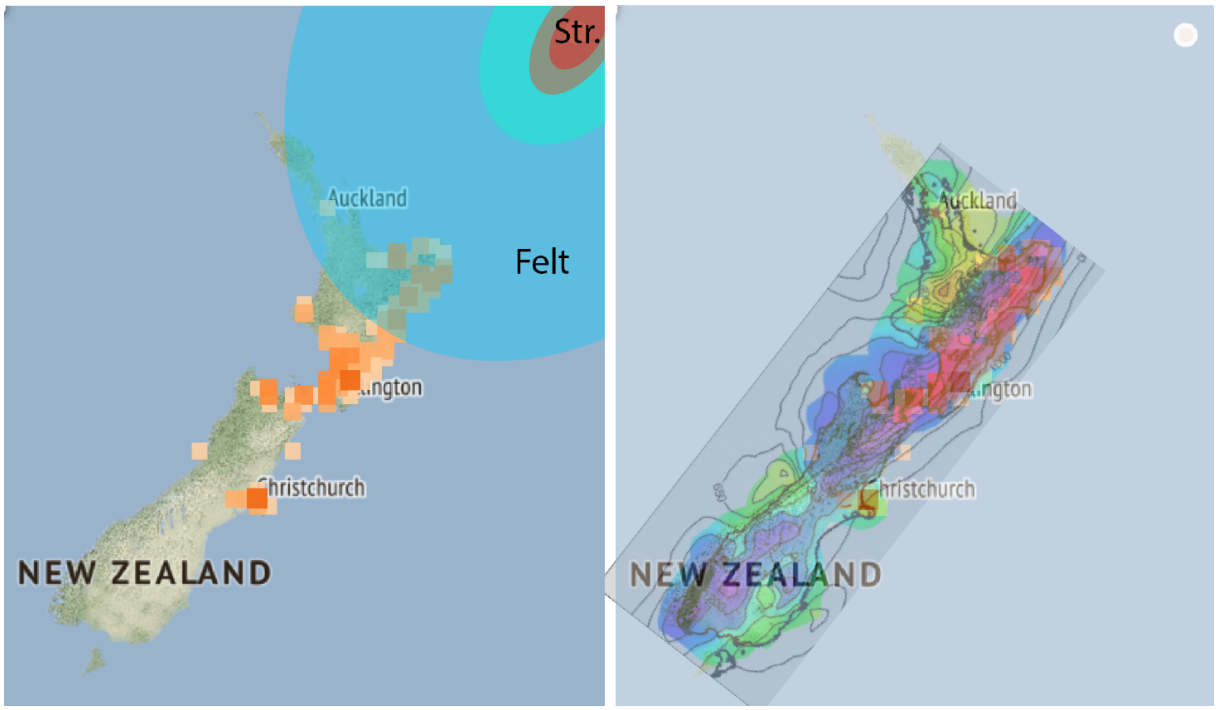

Figure 1.5 Left panel: Felt reports overlain by predicted regions of felt intensity from the September 2018 M6.9 Kermadec earthquake. Warmer colours show more intense shaking, cooler colours show less intense shaking. Note the lack of felt reports in the Auckland area and abundance of felt reports on the east coast of the North Island. Right panel has an overlay of the attenuation model of Eberhart-Phillips and Fry (2018). Note the strong correlation between regions of many felt reports and low attenuation (purple and red areas).

2.0 GROUND MOTION SIMULATIONS

To understand the effects presented in 1.1-1.3 as they relate to the utility of natural warning triggering, we systematically use a spectral element modelling scheme (AxiSEM, Nissen-Meyer et al., 2014) to simulate ground shaking in the North Island of New Zealand from scenario tsunamigenic earthquakes along the Kermadec subduction zone (Appendix 1). We present simulation results for M8.5 earthquakes at 2o intervals (approximately 220km) along the subduction zone and calculate resulting ground motions in Tauranga (Figure 2.1). We use Tauranga as an average proxy for the northern coast of the North Island, from the Bay of Plenty through the Auckland region. We calculate ground velocities to frequencies as high as 500 mHz.

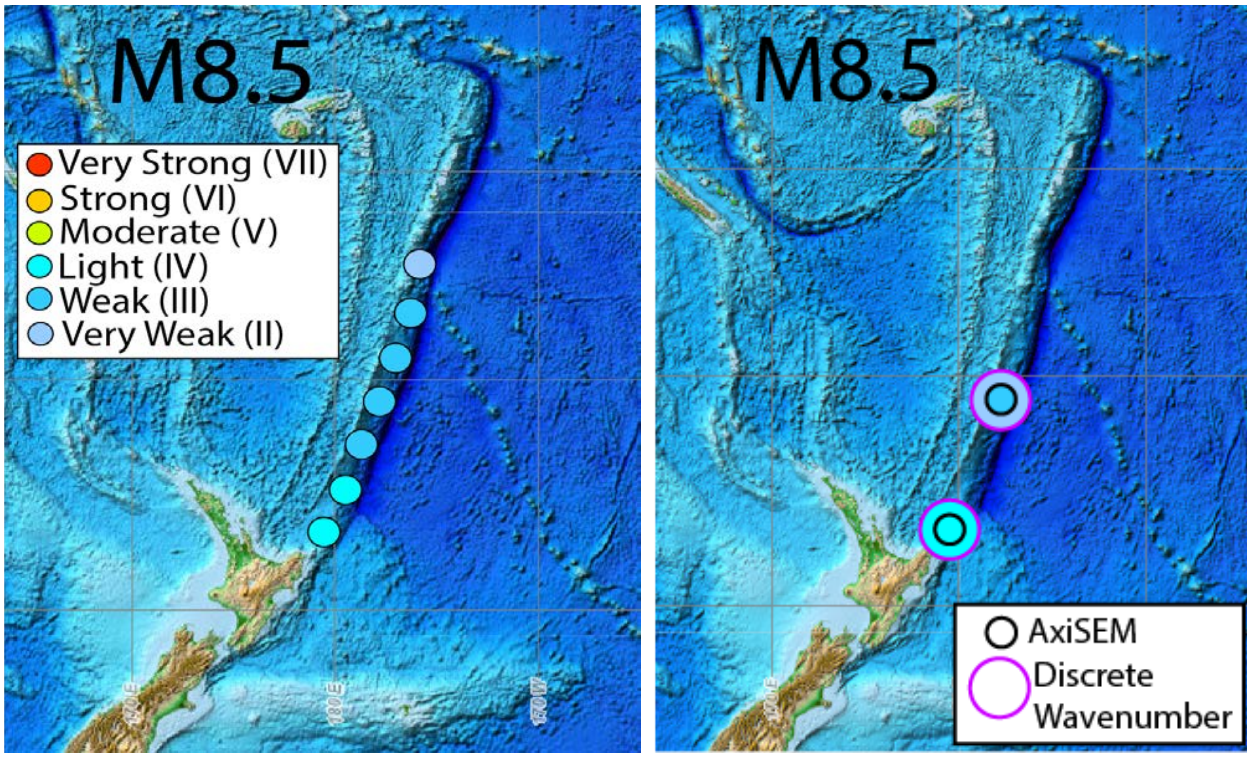

Figure 2.1 Left panel: Results from AxiSEM simulations of M8.5 earthquakes along the Kermadec Subduction zone. Earthquakes are located at each of the dots. The dots are colour-shaded according to their modelled felt intensities in Tauranga. Right panel: Comparison of AxiSEM results and two simulations with a discrete wavenumber numerical scheme.

We further test these ground motions against those calculated using a discrete wavenumber integration scheme (Bouchon and Aki, 1977) (Appendix 2). We use the same velocity and attenuation a-priori model as that implemented in the AxiSEM modeling. We model the most proximal event and a second event at ~1000 km. In both cases, the discrete wavenumber calculated ground velocities, although slightly smaller, are in general agreement with those calculated with the AxiSEM scheme (Figure 2.1).

We then compare the modelled ground motions with those predicted by recent ground motion prediction equations (Atkinson and Boore, 2003; Abrahamson et al, 2016; Zhao et al, 2006) (Figure 2.2). In each of these validation exercises, our synthetic calculations with AxiSEM lie within uncertainties or similar intensity classes as the compared data.

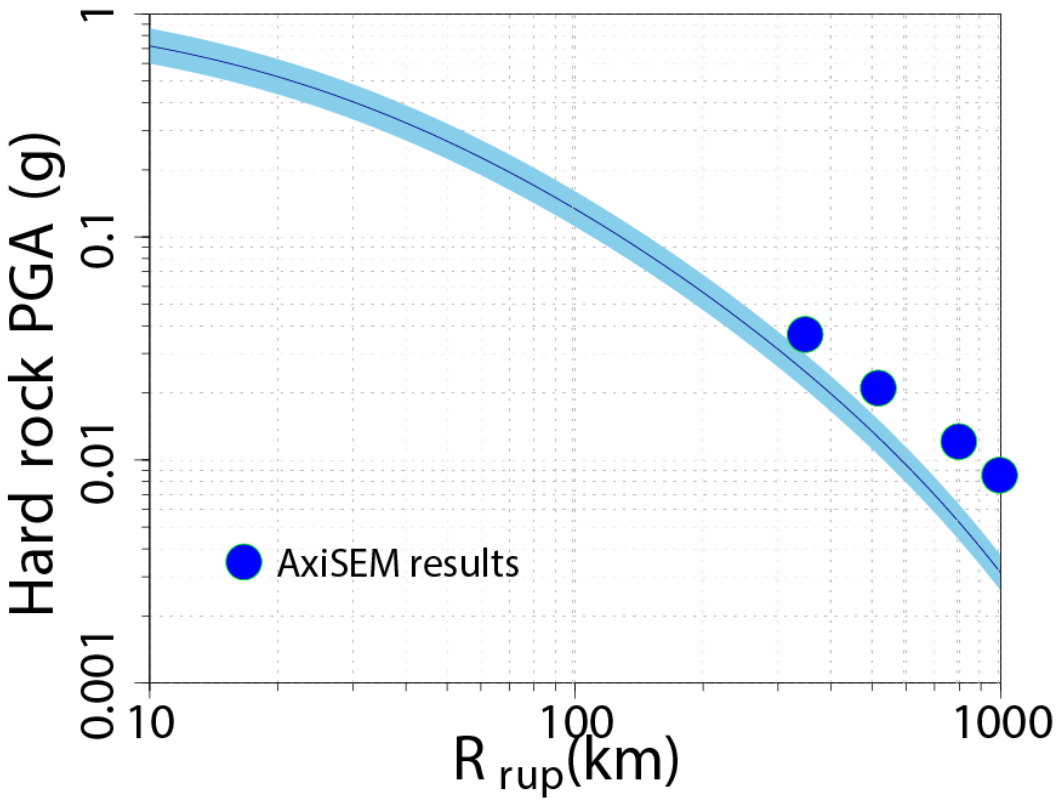

Figure 2.2 Comparison of our AxiSEM results with the recent ground motion prediction equation of Abrahamson et al., 2016. Results are within uncertainties of our numerical modelling given a simplified source model. Estimations of shaking for both of these techniques are compatible with the conclusion that these M8.5 events will not generate systematically strong shaking over most much of the north-western North Island. We note that recorded PGA has a wider bandwidth than simulated PGA, however, the relatively larger modelled ground motions suggest that we are capturing most important dominant frequencies at larger distances.

3.0 CONCLUSIONS

We use numerical simulations of ground motions from scenario earthquakes along the Kermadec subduction zone to test the limitations of the “Long or strong, get gone” self-evacuation through natural warning. These events are credible tsunami sources (> 5m at some coastal areas) yet their ground motions in the north-western North Island fall below the “strong” threshold resulting from felt intensity studies (Worden et al., 2012). While our synthetic models have significant uncertainty due to the unpredictable nature of the earthquake rupture process and subsequent wave propagation, they provide strong evidence for the inadequacy of natural warning alone to trigger evacuations in the northwestern North Island for significant tsunamigenic events as close as a few hundred kilometers from the New Zealand coast.

4.0 ACKNOWLEDGMENTS

We thank Chris Van Houtte for help with ground motion prediction equations and David Burbidge for insightful discussion.

5.0 REFERENCES

Abrahamson N, Gregor N, Addo K. 2016. BC Hydro ground motion prediction equations for ubduction earthquakes. *Earthquake Spectra*. 32(1):23-44.

Atkinson GM, Boore DM. 2003. Empirical ground-motion relations for subduction-zone earthquakes and their application to Cascadia and other regions. *Bulletin of the Seismological Society of America.* 93(4):1703-1729. doi:10.1785/0120020156.

Bouchon M, Aki K. 1977. Discrete wave-number representation of seismic source wave fields. *Bulletin of the Seismological Society of America.* 67(2):259–277.

Eberhart-Phillips D, Fry B. 2018 Joint local earthquake and teleseismic inversion for 3-D velocity and Q in New Zealand. *Physics of the Earth and Planetary Interiors. 283:*48-66. doi:10.1016/j.pepi.2018.08.005.

Nissen-Meyer T, van Driel M, Staehler SC, Hoseini K, Hempel S, Auer L, Colombi A, Fournier A. 2014. AxiSEM: broadband 3-D seismic wavefields in axisymmetric media. *Solid Earth*. 5:425-445. doi:10.5194/se-5-425-2014.

Power W, Wallace L, Wang X, Reyners M. 2012. Tsunami hazard posed to New Zealand by the Kermadec and southern New Hebrides subduction margins: an assessment based on plate boundary kinematics, interseismic coupling, and historical seismicity. *Pure and Applied Geophysics*. *169*(1-2):1-36.

Worden CB, Gerstenberger MC, Rhoades DA, Wald DJ. 2012. Probabilistic relationships between ground motion parameters and Modified Mercalli intensity in California. *Bulletin of the Seismological Society of America*. 102(1):204-221. doi:10.1785/0120110156.

Zhao JX, Zhang J, Asano A, Ohno Y, Oouchi T, Takahashi T, Ogawa H, Irikura K, Thio HK, Somerville PG, et al. 2006. Attenuation relations of strong ground motion in Japan using site classification based on predominant period. *Bulletin of the Seismological Society of America*. *96*(3):898-913. doi:10.1785/0120050122.

This page intentionally left blank.

APPENDICES

A1.0 NUMERICAL SIMULATIONS

A1.1 AxiSEM modelling

We use the parallel spectral element method "AxiSEM" (Nissen-Meyer et al., 2013) to generate the 3D wavefield of earthquakes along the Kermadec Subduction zone. This method solves the basic equation of motion in which the summation of mass and stiffnes terms are equivalent to the source term:

$$\overbrace{\int_{\oplus} \rho \boldsymbol{w} \cdot \partial_t^2 \boldsymbol{u}\, d^3\boldsymbol{x}}^{\text{mass term: } \mathbf{M}(\boldsymbol{u})} + \overbrace{\int_{\oplus} \nabla \boldsymbol{w} : \mathbf{C} : \nabla \boldsymbol{u}\, d^3\boldsymbol{x}}^{\text{stiffness term: } \mathbf{K}(\boldsymbol{u})} = \overbrace{\int_{\oplus} \boldsymbol{w} \cdot \mathbf{f}\, d^3\boldsymbol{x}}^{\text{source term: } \mathbf{F}(\boldsymbol{u})}$$

Where u is the displacement vector, w is a test vector, f is the source term, rho is the mass density and C is the elasticity tensor.

This approach expands the moment tensor response to mono-, di-, and quadropoles as displacement terms (u) relative to azimuth (ϕ):

u = u(s, z) , u = u(s, z) · f (sin φ, cos φ) , and u = u(s, z) · f (sin(2φ), cos(2φ)) , respectively, and convolves these with azimuthal radiation equations:

$$\boldsymbol{u}_m(\boldsymbol{x}) = \begin{pmatrix} u_s(\tilde{\boldsymbol{x}}) \cos m\phi \\ u_\phi(\tilde{\boldsymbol{x}}) \sin m\phi \\ u_z(\tilde{\boldsymbol{x}}) \cos m\phi \end{pmatrix}$$

Which provides the displacement wavefield at a point relative to the double-couple source. We solve the wave propagation within a velocity and attenuation model taken from Eberhart-Phillips and Fry, 2018 (Figure A1.1). We further take the time derivative of the displacement wavefield to generate 3D velocity wavefields from which we calculate the maximum velocity (Figure A1.2).

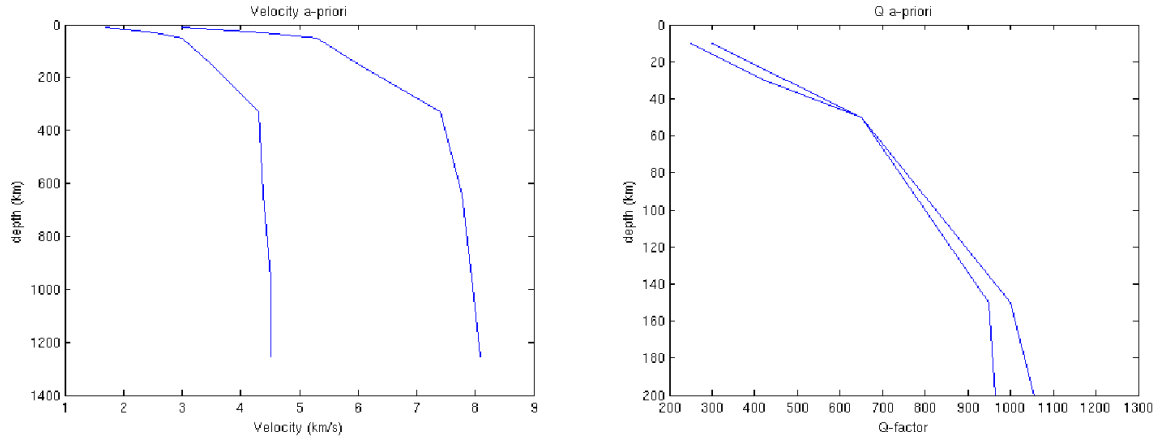

Figure A1.1 P and S velocity profiles (left panel) and Qp and Qs attenuation models (right panel) used in AxiSEM and discrete wavenumber numerical simulation.

We convert the maximum simulated ground velocity from these simulations within the USGS adopted “instrumental intensity” framework (Figure A1.3) to “Perceived Shaking”. Within this framework, we consider groundmotions > 9.6 cm/s strong and capable of triggering ‘long or strong, get gone’.

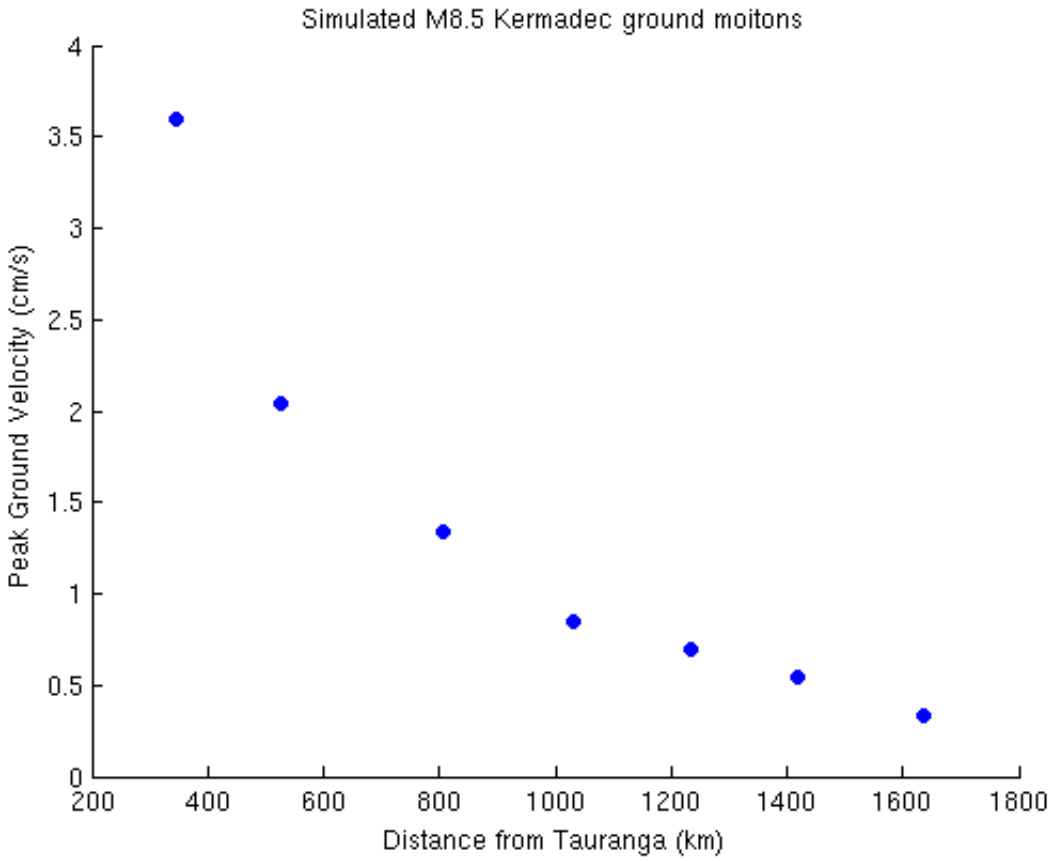

Figure A1.2 Peak ground velocity from our simulations as a function of distance from Tauranga.

PERCEIVED SHAKING	Not felt	Weak	Light	Moderate	Strong	Very strong	Severe	Violent	Extreme
POTENTIAL DAMAGE	none	none	none	Very light	Light	Moderate	Mod./Heavy	Heavy	Very Heavy
PEAK ACC.(%g)	<0.05	0.3	2.8	6.2	12	22	40	75	>139
PEAK VEL.(cm/s)	*<0.02*	*0.1*	*1.4*	*4.7*	*9.6*	*20*	*41*	*86*	*>178*
INSTRUMENTAL INTENSITY	I	II–III	IV	V	VI	VII	VIII	IX	X+

Scale based upon Worden et al. (2012)

Figure A1.3 Intensity table showing classification scheme used to assess perceived shaking against peak ground motions.

A1.2 Discrete Wavenumbermodelling

To test the results from the AxiSEM numerical simulations, we solve the analytical approach of Bouchon and Aki (1977). In this method, the 3-dimensional displacement vector (u) is the summation of displacement potentials (phi and psi) which are solutions to the wave equation in terms of P and S wave velocities alpha and beta, respectively:

$$\nabla^2\phi = \frac{1}{\alpha^2}\frac{\partial^2\phi}{\partial t^2} \qquad \nabla^2\psi = \frac{1}{\beta^2}\frac{\partial^2\psi}{\partial t^2}$$

By using body force equivalents to seismic dislocations, the displacement potentials of a double-couple source can be related to seismic moment through the integral relations

$$\phi = \frac{\mu D}{F}\int_0^L\int_0^W \left(\frac{\partial\phi^z}{\partial x_0} + \frac{\partial\phi^x}{\partial z_0}\right)\exp\left(-i\frac{\omega}{c}x_0\right)dx_0\,dy_0$$

$$\psi = \frac{\mu D}{F}\int_0^L\int_0^W \left(\frac{\partial\psi^z}{\partial x_0} + \frac{\partial\psi^x}{\partial z_0}\right)\exp\left(-i\frac{\omega}{c}x_0\right)dx_0\,dy_0$$

where uD, dxo, and dyo represent the seismic moment. By integrating these expressions, three components of displacement can be determined:

$$\phi = \frac{\mu D}{F}\int_0^L\int_0^W \left(\frac{\partial\phi^z}{\partial x_0} + \frac{\partial\phi^x}{\partial z_0}\right)\exp\left(-i\frac{\omega}{c}x_0\right)dx_0\,dy_0$$

$$\psi = \frac{\mu D}{F}\int_0^L\int_0^W \left(\frac{\partial\psi^z}{\partial x_0} + \frac{\partial\psi^x}{\partial z_0}\right)\exp\left(-i\frac{\omega}{c}x_0\right)dx_0\,dy_0$$

$$w = \frac{-D}{2L_xL_yk_\beta^2}\sum_{n_x}\sum_{n_y}k_x\left(-2\nu e^{-i\nu|z|} + \frac{\gamma^2 - k_x^2 - k_y^2}{\gamma}e^{-i\gamma|z|}\right)$$

$$\cdot\frac{\exp(ik_xL - i\omega/cL) - 1}{\omega/c - k_x}\,\frac{\exp(ik_yW) - 1}{k_y}\exp(-ik_xx - ik_yy)$$

These are of course frequency domain solutions. They can be turned into time-domain displacement seismograms. For our Kermadec megathrust case, the full reflected and transmitted wavefields can be found by discrete equations for P, SV, and SH as:

$$\phi(k_x, k_y) = \frac{iD}{L_x L_y k_\beta^2}\left[\sin\theta\cos\theta\left(\frac{k_y^2}{\nu} - \nu\right)\right.$$

$$\left. + (\sin^2\theta - \cos^2\theta)k_y\right]\left[\frac{\exp(ik_x W) - 1}{k_x}\right.$$

$$\left. \cdot \frac{\exp(ik_y L\cos\theta - i\omega/cL - i\nu z_1) - \exp(-i\nu z_0)}{\omega/c - k_y\cos\theta - \nu\sin\theta}\right]$$

$$\cdot \exp(-ik_x x - ik_y y + i\nu z) \qquad (25)$$

$$\psi^{SV}(k_x, k_y) = \frac{iD}{2L_x L_y k_\beta^2}\frac{1}{k}\left[2\sin\theta\cos\theta(k_x^2 + 2k_y^2)\right.$$

$$\left. + (\sin^2\theta - \cos^2\theta)\frac{k_y}{\gamma}(\gamma^2 - k_x^2 - k_y^2)\right]\left[\frac{\exp(ik_x W) - 1}{k_x}\right.$$

$$\left. \cdot \frac{\exp(ik_y L\cos\theta - i\omega/cL - i\gamma z_1) - \exp(-i\gamma z_0)}{\omega/c - k_y\cos\theta - \gamma\sin\theta}\right]$$

$$\cdot \exp(-ik_x x - ik_y y + i\gamma z)$$

$$V^{SH}(k_x, k_y) = \frac{D}{2L_x L_y k_\beta^2}\frac{k_x k_\beta^2}{k}\left[2\sin\theta\cos\theta\frac{k_y}{\gamma}\right.$$

$$\left. + [\sin^2\theta - \cos^2\theta)]\left[\frac{\exp(ik_x W) - 1}{k_x}\right.\right.$$

$$\left.\left. \cdot \frac{\exp(ik_y L\cos\theta - i\omega/cL - i\gamma z_1) - \exp(-i\gamma z_0)}{\omega/c - k_y\cos\theta - \gamma\sin\theta}\right]\right.$$

$$\cdot \exp(-ik_x x - ik_y y + i\gamma z)$$

where y and z are location terms and l and theta are geometric terms of the source fault.

Lastly, we apply the attenuation to generate 3-component displacement waveforms for select scenarios.

Figure A2.1 presents the 3-component velocity wavefield for an M8.5 with identical source parameters to the southernmost scenario considered with AxiSEM.

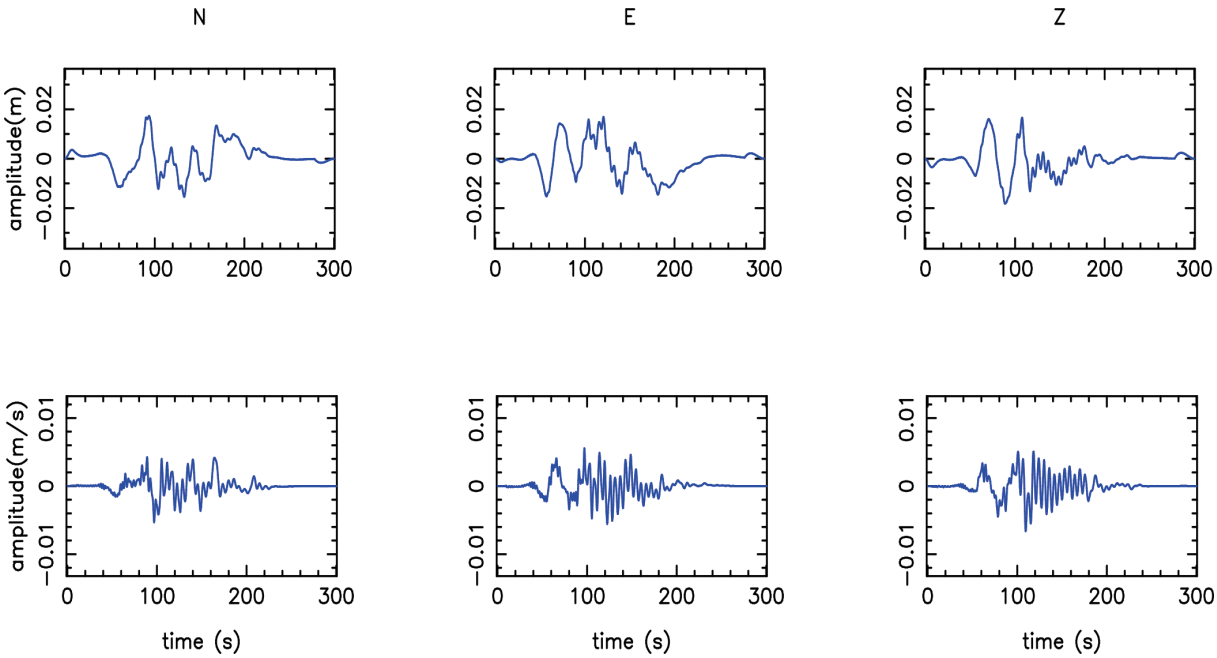

Figure A1.4 Results of the southernmost M8.5 simulation shown in Figure 2.1. Top row is the 3-component displacement wavefield. Bottom row is the velocity wavefield used for comparison with AxiSEM results.